Processing and Application of Ceramics 12 [3] (2018) 277–286
https://doi.org/10.2298/PAC1803277A

Electrochemical performance of sol-gel derived $La_{0.6}Sr_{0.4}CoO_{3-\delta}$ cathode material for proton-conducting fuel cell: A comparison between simple and advanced cell fabrication techniques

Abdullah Abdul Samat[1], Wan Nor Anasuhah Wan Yusoff[1], Nurul Akidah Baharuddin[1], Mahendra Rao Somalu[1,*], Andanastuti Muchtar[1,2], Nafisah Osman[3]

[1]*Fuel Cell Institute, Universiti Kebangsaan Malaysia, 43600 UKM Bangi, Selangor, Malaysia*
[2]*Centre for Materials Engineering and Smart Manufacturing (MERCU), Faculty of Engineering and Built Environment, Universiti Kebangsaan Malaysia, 43600 UKM Bangi, Selangor, Malaysia*
[3]*Faculty of Applied Sciences, Universiti Teknologi MARA, 02600 Arau, Perlis, Malaysia*

Received 17 April 2018; Received in revised form 3 August 2018; Accepted 21 August 2018

Abstract

In this study, the effects of different fabrication techniques on the electrochemical performance of sol-gel derived $La_{0.6}Sr_{0.4}CoO_{3-\delta}$ (LSC) cathode material for intermediate temperature proton-conducting fuel cells were investigated. Single-phase, sub-micron LSC powder was used to prepare cathode slurries by a simple grinding-stirring (G-S) technique and an advanced ball milling-triple roll milling (BM-TRM) technique. The prepared G-S and BM-TRM cathode slurries were brush painted and screen printed, respectively, onto separate $BaCe_{0.54}Zr_{0.36}Y_{0.1}O_{2.95}$ (BCZY) proton-conducting electrolytes to fabricate symmetrical cells of LSC|BCZY|LSC. The thickness of LSC cathode layer prepared by brush painting and screen printing was 17 ± 0.5 μm and 7 ± 0.5 μm, and the surface porosity of the layers was 32% and 27%, respectively. Electrochemical impedance spectroscopy analysis revealed that the layer deposited by screen printing had lower area specific resistance measured at 700 °C (0.25 Ω cm^2) than the layer prepared by brush painting of G-S slurry (1.50 Ω cm^2). The enhanced LSC cathode performance of the cell fabricated using BM-TRM assisted with screen printing is attributed to the improved particle homogeneity and network in the prepared slurry and the enhanced particle connectivity in the screen printed film.

Keywords: *LSC cathode, SOFC, brush painting, screen printing, polarization resistance*

I. Introduction

Solid oxide fuel cell (SOFC) is an electrochemical device that directly converts the chemical energy of a fuel to the electrical energy through electrochemical reactions. Reducing the operating temperature of SOFCs from high (800–1000 °C) to intermediate (500–800 °C) temperature is a main target in the present SOFC research. Hence, cost reduction and wider material choices for cell components are obtained [1,2]. However, high cathode polarization resistance (R_p) at reduced temperature limited the performance of SOFC [3–5]. Thus, the development of promising cathode materials, particularly for intermediate-temperature proton-conducting SOFC or the proton-conducting fuel cell (PCFC), remains a challenging task.

The most promising cathode materials are cobalt-containing perovskite-type oxide materials such as strontium-doped lanthanum cobaltite ($La_{0.6}Sr_{0.4}CoO_{3-\delta}$, LSC). LSC showed good performance at the intermediate-temperature [3,6–9]. Our previous work [10] reported that the cathode polarization resistance (R_p) in terms of area specific resistance (ASR) of the LSC cathode working on yttrium-doped barium cerate-zirconate ($BaCe_{0.54}Zr_{0.36}Y_{0.1}O_{2.95}$, BCZY) proton conductor at 700 °C was 0.48 Ω cm^2. Although the ASR value is comparable to those in other reported works in the literature, the value is considered higher than those of other cobalt-containing cathode materials [2,4,11]. Therefore, the present work

*Corresponding authors: tel: +6 03 8911 8522,
fax: +6 03 8911 8530, e-mail: *mahen@ukm.edu.my*

aims to improve the electrochemical properties of the LSC cathode for application in BCZY-based PCFC at intermediate-temperature by reducing the ASR value.

Many approaches were adopted to reduce Rp of cathode materials; including the use of composite cathode [9], modification of cathode structure from ABO_3 to ABO_4 [12], addition of dopant material [13], and variation of synthesis routes to optimize the cathode microstructure [14]. All these approaches mainly focused on the synthesis or production of cathode materials. Moreover, the designing and controlling cell fabrication parameters are regarded as promising approaches to reduce R_p. These approaches aided in optimizing the cathode structure on the electrolyte by reducing the deleterious effect upon transport of charge carrier species [15,16]. In the cell fabrication technique, most of the works reported on the effects of thickness, porosity, and sintering temperature on R_p of the printed cathode layer or film [17–19]. Nevertheless, the studies on the effects of different slurries or ink preparations and slurry deposition techniques on the electrochemical properties of cathode materials are limited. The optimization of slurry properties and cathode structure by different slurry preparations and slurry deposition techniques is also important to produce defect-free sintered films with desired electrical and electrochemical performances [20–23]. Thus, this study evaluated the effects of different slurry preparation and deposition techniques on the electrochemical properties of LSC cathode.

In the present study, the LSC powder was synthesized using a sol-gel method. Grinding-stirring (G-S) and ball milling-triple roll milling (BM-TRM), respectively, were used to prepare LSC cathode slurries. G-S is the simplest and time-effective technique to produce cathode slurry in a small-scale research laboratory [24–26]. This approach is also cost effective technique because it requires inexpensive apparatus or instruments. Conversely, BM-TRM is an advanced technique because it involves considerable high-end and sophisticated instruments. BM-TRM is considered as a promising technique in preparing a homogeneous ink or slurry [20]. To fabricate the symmetrical cells of LSC|BCZY|LSC, the prepared cathode slurries are deposited separately onto the surfaces of BCZY electrolyte pellets by brush painting and screen printing, which are simple and advanced cell fabrication techniques, respectively. Both techniques were extensively used to fabricate thin films [4,10,21,27,28]. Screen printing technique can effectively control the thickness of printed film unlike brush painting [20]. The electrochemical performance of the fabricated symmetrical cells at working temperature of 700 °C is evaluated using an electrochemical impedance spectroscopy (EIS) instrument. The present results may provide a significant knowledge in optimizing and improving the overall cell fabrication process to produce LSC cathode with high performance and a low ASR value for intermediate-temperature PCFC application.

II. Experimental

2.1. Powder synthesis and characterization

$La_{0.6}Sr_{0.4}CoO_{3-\delta}$ (LSC) powder was prepared via a sol-gel method. High purity (> 99%) metal nitrate salts of lanthanum ($La(NO_3)_3 \cdot 6\,H_2O$), strontium ($Sr(NO_3)_2$) and cobalt ($Co(NO_3)_2 \cdot 6\,H_2O$) were purchased from Acros (Belgium) and used as starting materials. A metal nitrate salt solution was prepared by dissolving a stoichiometric amount of the starting materials in 100 ml of deionized water. When the starting materials were completely dissolved in the deionized water, stoichiometric amounts of citric acid monohydrate (99.5% purity, Merck) and ethylenediaminetetraacetic acid (EDTA, 99% purity, Acros) were added into the metal nitrate salt solution. Afterwards, the solution pH was adjusted to 0.5 [6]. Finally, a stoichiometric amount of ethylene glycol (EG, 99.97% purity, Acros) was added and the solution mixture was continuously stirred and heated for several hours until a viscous gel was formed. The obtained viscous gel was dried at 150 °C for 12 h and at 250 °C for 5 h. The precursor powder was calcined at 900 °C for 5 h with a heating/cooling rate of 5 °C/min. Details for the production of the LSC powder are described elsewhere [10].

Thermogravimetric analyser (SDT-Q600, TA instrument, USA) was used to study the thermal decomposition behaviour of the precursor powder in the temperature range of 30–1200 °C at a heating rate of 10 °C/min and in flowing purified air with a flow rate of 100 ml/min. X-ray diffractometer (XRD, Bruker D8-Advance, Germany) using Cu-K_α radiation source (λ = 0.1540558 nm) was utilized to confirm the formation of LSC perovskite phase. The XRD was operated at 40 kV and 40 mA for the 2θ ranging from 20° to 80° at a scan rate of 0.025°/step. The specific surface area of the calcined powder was measured by surface area and porosimetry system (Micromeritics, ASAP 2020, USA) using Brunauer-Emmett-Teller (BET) technique. The calcined powder morphology was examined by a scanning electron microscope (SEM, Zeiss Merlin, Germany). The mean particle size was estimated by statistical analysis on 100 particles in the SEM images using ImageJ software.

2.2. Slurry preparation

Grinding-stirring (G-S) technique

The calcined LSC powder was ground in an agate mortar for 10 min. Subsequently, ethyl cellulose (EC) as a binder and terpineol as a solvent were mixed with the obtained powder and continuously ground in the agate mortar for another 10 min. Afterwards, the mixture was transferred into a 50 ml beaker and stirred on a hotplate with stirrer using a magnetic bar for 1 h to produce LSC cathode slurry.

Ball milling-triple roll milling technique

The calcined LSC powder was mixed with acetone as a solvent and Hypermer KD15 (Croda International, UK) as a dispersant. The mixture was ball milled in a zirconia jar using zirconia balls (diameter of 10 mm) for 5 h. The zirconia ball-to-LSC powder ratio was 4 : 1. The ball milled LSC powder was dried in an oven at 90 °C for 6 h. The dried powder was mixed with EC in terpineol and ground in an agate mortar for 10 min. The mixture was milled using a triple roll mill for 30 min to produce homogeneous LSC cathode slurry.

2.3. Symmetrical cell fabrication and characterization

A single-phase BCZY powder was prepared using a sol-gel method [29]. The prepared powder was pressed into pellets (diameter of 13 mm) under isostatic pressing using a uniaxial pressing machine (Carver, Model: 4350 L, IN, USA) at a loading force of 5 tons for 1 min. The as-prepared green pellets were sintered at 1400 °C for 10 h using a high-temperature chamber furnace to densify the pellets. The surfaces of the sintered pellets were polished using #1000 grit paper. These pellets were ultrasonically cleaned to remove contaminants from the polished surfaces. The LSC cathode slurries prepared by G-S and BM-TRM techniques were deposited onto the surfaces of the polished pellets by brush painting and screen printing, respectively, to produce the symmetrical cells of LSC|BCZY|LSC. The produced symmetrical cells were sintered at 900 °C for 2 h. The fabricated symmetrical cells were denoted as S1 (G-S, brush painted) and S2 (BM-TRM, screen-printed).

Microstructure images of the cross-section and surface of the symmetrical cells were taken by a SEM (Hitachi U1510, Japan). These images were also used to measure the thickness and porosity (by adjusting the threshold) of the LSC cathode layer using ImageJ software. The electrochemical properties of the fabricated symmetrical cells were determined on the basis of the electrochemical impedance spectroscopy (EIS) results. The EIS measurement was performed on ZIVE SP2 electrochemical workstation (ZIVELAB WonATech, Korea) at 700 °C in humidified air over the frequency range of 0.1 Hz–1 MHz with a low-amplitude sinusoidal voltage of 20 mV under open circuit conditions. Data acquired from the EIS measurement were analysed using a ZMAN™ 2.2 f3 (ZIVE LAB) software. The impedance diagrams were plotted in real impedance (Z') versus imaginary impedance (Z''). The area specific resistance (ASR) was calculated using the following equation: $ASR = (R_p \times A)/2$, where R_p refers to the resistance or polarization resistance at cathode|electrolyte interface, and A refers to the specific active area (0.50 cm^2).

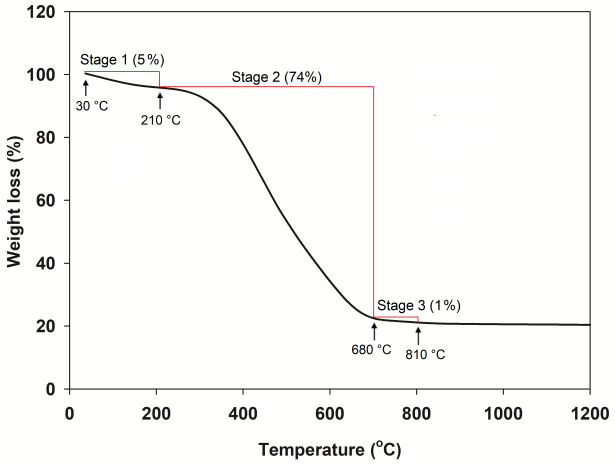

Figure 1. Thermogravimetric plot of $La_{0.6}Sr_{0.4}CoO_{3-\delta}$ (LSC) precursor powder

III. Results and discussion

3.1. Powder characterization

Figure 1 shows the thermogravimetric analysis plot of the LSC precursor powder dried at 250 °C. The plot indicates three stages of weight loss with the total weight loss of ~80%. An initial weight loss of ~5% observed at stage 1 in the temperature region of 30–210 °C is associated with the dehydration of absorbed moisture, traces of structural hydroxide (−OH) and decomposition of the remaining organic compounds with low boiling point such as citric acid (175 °C) and EG (197 °C), in the precursor powder. The major weight loss of ~74% is observed at 210–680 °C (stage 2). This weight loss is attributed to the decomposition of residual nitrates and organic compounds (citric acid, EDTA and EG) in the sample [29,30]. A minor weight loss of ~1% at stage 3 (680–810 °C) is caused by the decomposition of trapped carbonaceous residue, which are formed as intermediate products after the combustion of organic compounds [6,31]. After stage 3, the plot presents a plateau with no further weight loss, which indicates the beginning of crystallization and structural transformation to form the desired oxide materials [32]. Thus, 810 °C is recommended as the minimum calcination temperature.

According to the thermogravimetric analysis results, the as-synthesized powder is calcined at 900 °C (slightly higher than the recommended minimum calcination temperature). Figure 2 presents the XRD pattern of the calcined powder. The pattern confirmed that the calcined powder forms a single LSC perovskite phase because all the peaks in the XRD pattern are matched with the ICDD reference code 00-048-0121 with a cubic $Pm{-}3m$ structure. The pronounced peaks are indexed using the following Miller indices: (100), (110), (111), (200), (211), (220), (300), and (310). This result is consistent with our previous reported work [10] and comparable to those of other reported studies in the literature for LSC material [6,7,31,33].

Typical particle morphology of the calcined LSC powder is shown in Fig. 3. The powder is made up of homogeneous and almost identical particles with regu-

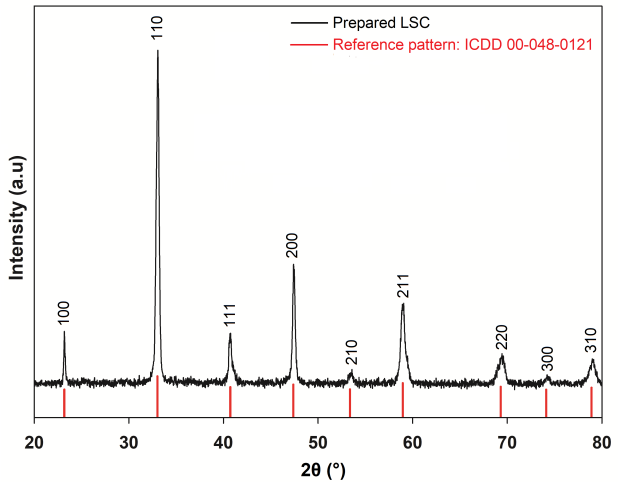

Figure 2. XRD pattern of $La_{0.6}Sr_{0.4}CoO_{3-\delta}$ (LSC) powder calcined at 900 °C for 5 h

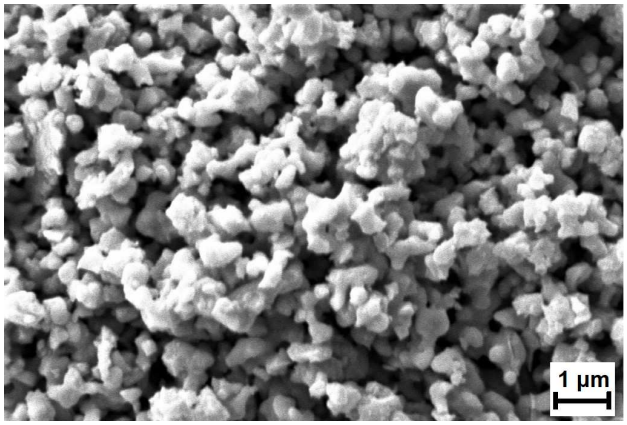

Figure 3. SEM image of $La_{0.6}Sr_{0.4}CoO_{3-\delta}$ (LSC) powder calcined at 900 °C for 5 h

lar shape. The particles are loosely agglomerated and connected with one another. The major disadvantage of wet chemical methods, including sol-gel method, is the agglomeration of the ultrafine crystallites or particles. The mean particle size and BET specific surface area of the calcined powder are 0.28 ± 0.06 µm and 8.7 m^2/g, respectively. Although the mean particle size of the LSC produced in this work is larger than that of the LSC powder produced by citric acid-EDTA complexation assisted with polyethylene glycol as surfactant with a nano-size of 60 nm [6], its BET specific surface area is slightly larger than that of the nano-size powder (8.22 m^2/g). The same observation was also reported by Benel *et al.* [34]; they prepared a LSC powder by salt-assisted spray pyrolysis and obtained a high BET specific surface area (60 m^2/g) and particle size diameter of 0.5–5 µm. Thus, a powder with a large surface area can be obtained by various synthesis methods regardless of the particle size.

3.2. Characterization of the fabricated cell

Homogeneous cathode layer on the electrolyte substrate with uniform thickness (7 ± 0.5 µm) was prepared by screen printing, as a simple and economic technique (the sample S2 Fig. 4). The homogeneous and well-dispersed particle distribution with 27% surface porosity could significantly improve the electrochemical performance of the LSC cathode. In contrast, the fabrication of S1 cathode layer on the electrolyte substrate through brush painting using the non-homogeneous slurry resulted in a non-homogeneous particle distribution with 32% surface porosity and non-uniform thickness (17 ± 0.5 µm) of S1 cathode layer (Fig. 5). This non-uniform particle distribution could lower the electrochemical performance of the LSC cathode.

3.3. Electrochemical properties analysis

The typical EIS spectra for the symmetrical S1 and S2 cells in the frequency ranging from 0.1 Hz to 50 kHz measured at 700 °C are depicted in Figs. 6a and 6b, respectively. The impedance spectra consist of two arcs, which indicate that at least two responses corresponding to the electrolyte and/or electrode (cathode) reactions occur. The equivalent circuit model in Fig. 6c was used to fit and analyse the impedance spectra. R_s, R_1, R_2 and R_3 are resistances and Q_1, Q_2 and Q_3 are constant phase elements (CPEs), also be regarded as pseudo-capacitances. The resistances and CPEs values obtained

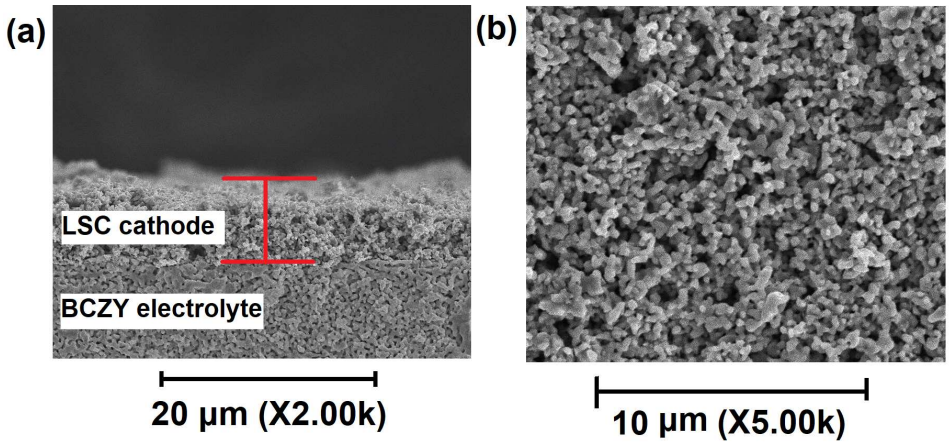

Figure 4. SEM images of the cross-section (a) and the surface (b) of the symmetrical cell fabricated by ball milling-triple roll milling assisted with screen printing

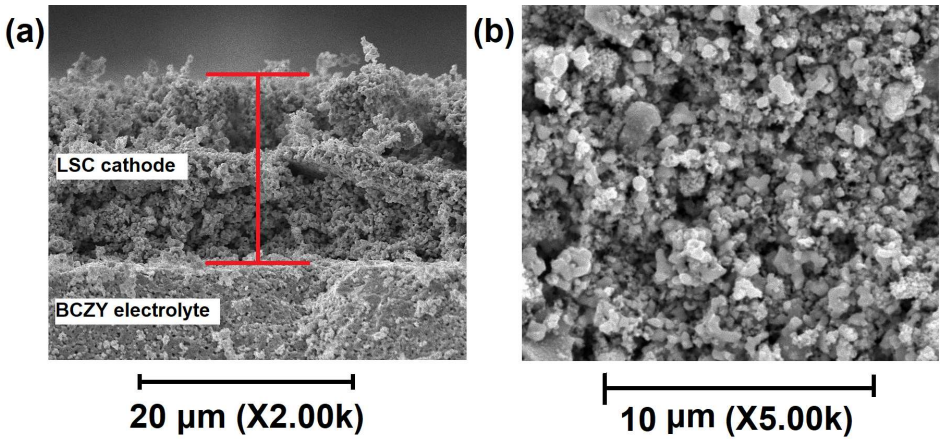

Figure 5. SEM images of the cross-section (a) and the surface (b) of the symmetrical cell fabricated by grinding-stirring assisted with brush painting

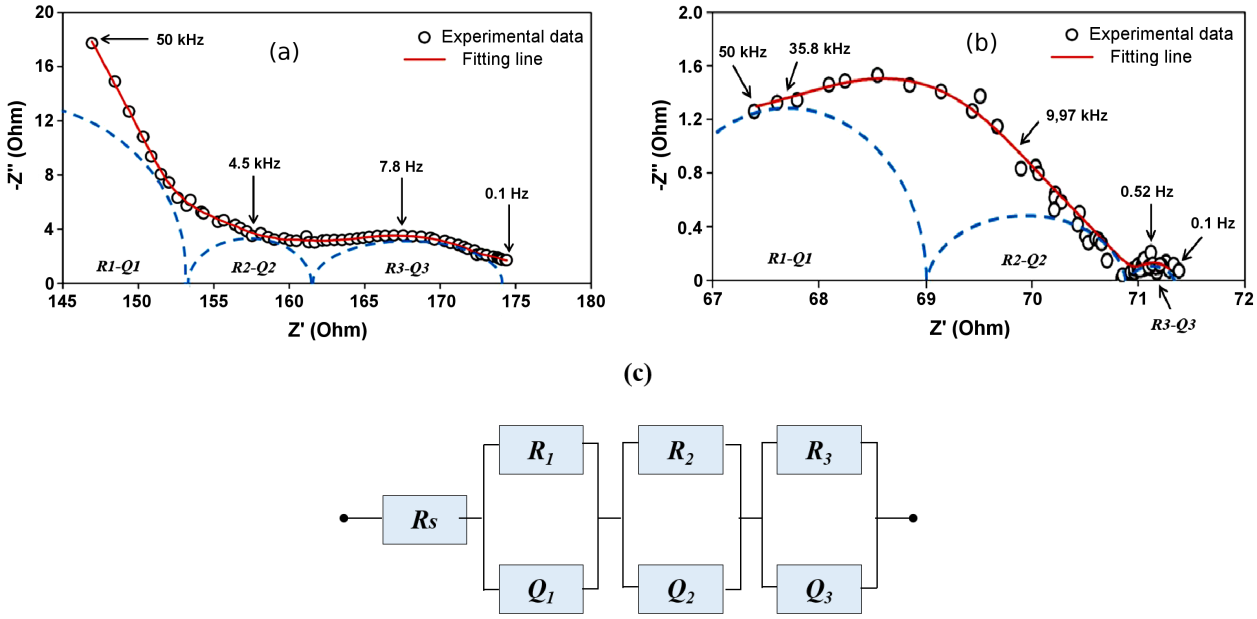

Figure 6. Impedance spectra and fitted results of S1 (a) and S2 (b) symmetrical cells measured at 700 °C and adopted equivalent circuit model (c)

from the fitting process were directly used to calculate the capacitance (C) and characteristic frequency (f_{max}) values by using the following equations:

$$C = Y^{\frac{1}{n}} \cdot R^{\frac{1}{n-1}} \quad (1)$$

$$f_{max} = \frac{1}{2\pi \cdot R \cdot C} \quad (2)$$

where Y and n are the parameters related to the CPEs and R is the resistance. The calculated values of C and f_{max} are tabulated in Table 1.

R_s represents the ohmic resistance, which is associated with the electrolyte and electrical contacts. R_1-Q_1 represents the grain-boundary response from BCZY electrolyte. In mixed ionic-electronic conductors, such as LSC cathode, the oxygen reduction reaction can occur at cathode|electrolyte interface and in the bulk of cathode material. R_2-Q_2 corresponds to the charge transfer process associated with O^{2-} ion incorporation at the cathode|electrolyte interface and the surface diffusion of O^{2-} ion throughout the bulk cathode (cathode thickness) [19]. R_3-Q_3 corresponds to the oxygen surface ex-

Table 1. Capacitance and characteristic frequency values for equivalent circuits of symmetrical S1 and S2 cells measured at 700 °C

Symmetrical cell	Capacitance, C [F]			Frequency, f_{max} [Hz]		
	Q_1	Q_2	Q_3	R_1-Q_1	R_2-Q_2	R_3-Q_3
S1	$2.67 \cdot 10^{-9}$	$3.20 \cdot 10^{-6}$	$1.20 \cdot 10^{-3}$	$4.38 \cdot 10^{5}$	$4.50 \cdot 10^{3}$	7.80
S2	$7.84 \cdot 10^{-7}$	$2.51 \cdot 10^{-5}$	$7.86 \cdot 10^{-1}$	$3.58 \cdot 10^{4}$	$9.97 \cdot 10^{3}$	0.521

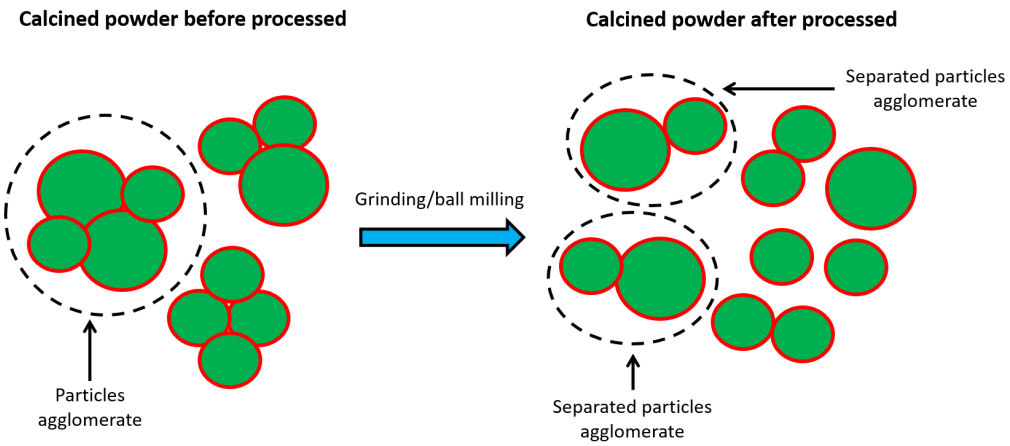

Figure 7. Proposed illustrations for the breaking down of particle agglomerates by grinding and ball milling techniques

change process involving the dissociation/adsorption of oxygen at the cathode surface, reduction of the adsorbed oxygen, and incorporation of O^{2-} ion into the LSC cathode at low-frequency region [35–37]. Since the R_1 corresponds to the electrolyte response, then only R_2 and R_3 are used to calculate the ASR values.

The ASR values of the LSC cathode for the symmetrical S1 and S2 cells measured at 700 °C are 1.50 and 0.25 Ω cm^2, respectively. A factor that contributed to the low ASR value in the symmetrical S2 cell was the formation of uniform screen-printed LSC cathode layer as illustrated in Fig. 4. It is important to note that the use of combined ball milling-triple roll milling (BM-TRM) technique significantly reduced the particle agglomerates in the prepared LSC cathode slurry and resulted in homogeneous slurry. The LSC cathode layer fabricated by screen printing process using the homogeneous slurry resulted in a cathode layer with uniform particle distribution. This explained the reason for the low ASR value in the symmetrical S2 cell. Conversely, the high ASR value in the symmetrical S1 cell can be related to the non-homogeneous distribution of particles in the LSC cathode slurry produced by simple grinding-stirring (G-S) technique. Some of the particle agglomerates cannot be further broken into smaller particles through this technique. As a result, the cathode slurry was non-homogeneous and the distribution of particles in the resultant cathode layer was non-uniform as confirmed in Fig. 5. This is probably a good reason for the high ASR value measured using the symmetrical S1 cell.

3.4. Discussion - Influence of fabrication process

At the first stage of the cathode slurry preparation, the calcined LSC powders were respectively subjected to the grinding and ball milling techniques in order to reduce particle agglomerates. Grinding and milling processes are considered important in the preparation of slurries because their use can lead to the uniform dispersion and particle size reduction. Having a uniform particle dispersion with reduced size is a prerequisite for the fabrication of a homogeneous porous structure of cathode film with uniformly distributed pores [38]. Generally, both grinding and ball milling reduce the size of particle agglomerates by mechanical action. Pressure is applied during the mechanical action and the particles are subjected to a stress. Under the stress, some crashes will occur, subsequently the particle agglomerates will be broken and their size will be reduced (Fig. 7). The particle size of the powders subjected to the ball milling is lower than that of those subjected to the grinding as reported by Oda *et al.* [23]. However, the processed powders with the reduced particle size could still result in inhomogeneity [39].

At the second stage, the ground, ball milled and calcined LSC powders were further processed by stirring and triple roll milling techniques, respectively. The proposed illustrations for the breaking down of particle agglomerates by stirring and triple roll milling techniques are illustrated in Fig. 8. The stirring process can only maintain the slurry homogeneity rather than the agglomerate breaking. During the stirring process, it can be observed that the small particles accumulated at the centre of the beaker while the big particles deposited on the edge of the beaker. This can result in non-homogeneous slurry and the fabricated film using this slurry has non-uniform particle distribution (Fig. 5). However, the use of the triple roll mill in the preparation of slurry can result in homogeneous slurry with uniform particle distribution. Triple roll mill can also significantly reduce particle agglomeration in the prepared slurry. The triple roll mill is equipped with three rolls turning in opposite directions. In the triple roll milling, the inhomogeneous slurry is fed between the rollers 1 and 2 having a gap of 15 μm as shown in Fig. 8b. The slurry is exposed to compression and shear forces when it passes through the gap. In this stage, the majority of the agglomerates in the slurry will be broken to smaller agglomerates. The slurry with reduced agglomerates is then passed through a smaller gap (5 μm) between rollers 2 and 3 for further breakage of particle agglomerates before recovering a final homogeneous slurry via roller 3.

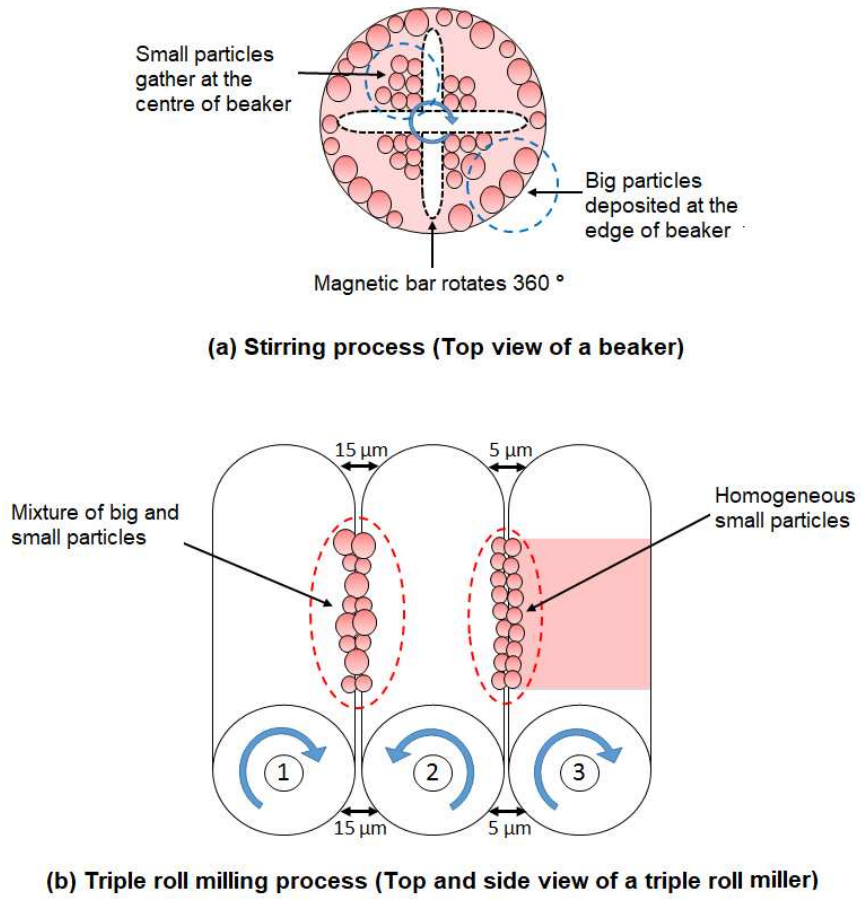

Figure 8. Proposed illustrations for the breaking down of particle agglomerates by stirring (a) and triple roll milling (b)

Particles with homogeneous size in the cathode film S2 resulted in a lower resistance than that of the cathode film S1 with non-homogeneous particle size as illustrated in Fig. 9. It is expected that particles with homogeneous size have a larger direct contact and/or grain boundary contact area between particles, which then allows better ionic current flow. Conversely, smaller direct contact area represents a constriction which hinders the ionic flow and consequently leads to an additional, resistive grain boundary contribution in an impedance

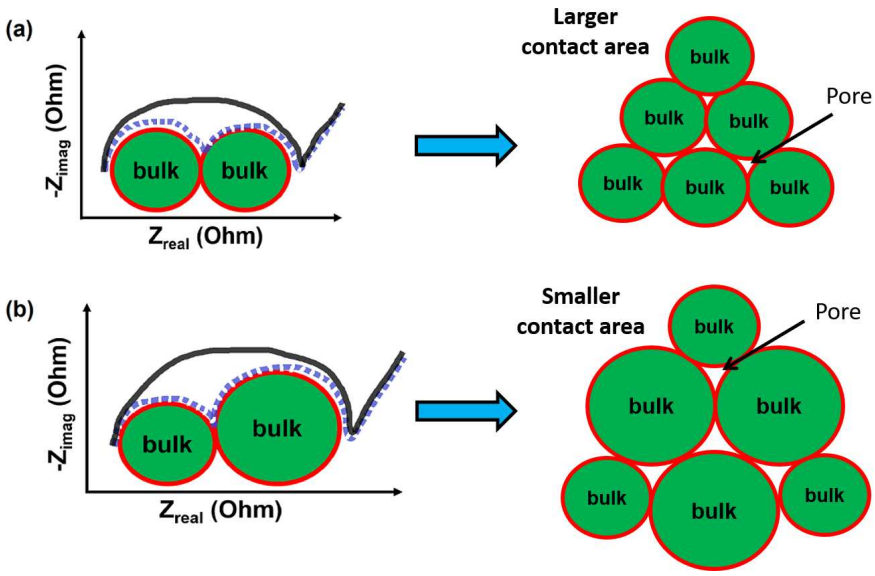

Figure 9. Proposed illustrations for the effects of homogeneous (a) and non-homogeneous (b) particles on the polarization resistance (adopted from [40])

Table 2. *ASR* values of LSC cathode prepared and fabricated by different techniques with various electrolytes measured at 700 °C

Synthesis method	Fabrication method	Electrolyte	ASR [$\Omega\,cm^2$]	Reference
Solid state reaction	Screen printing	SDC20	1.08	[33]
Glycine-nitrate	Screen printing	GDC	2.0	[41]
Polymeric complexation	Brush painting	BCZY	0.48	[10]
Commercial powder	Pulsed laser deposition	YSZ	0.3	[42]
Sol-gel	Brush painting	BCZY	1.50	This work
Sol-gel	Screen printing	BCZY	0.25	This work

spectrum [40]. This observation is in line with the results of film porosity in which the larger direct contact area is less porous than the smaller direct contact area.

Overall, in this work, the advanced BM-TRM technique assisted with screen printing produced LSC powder with improved performance compared to the cathode produced using G-S technique assisted with brush painting. The ability of the simple and cost-effective techniques in producing a comparable electrochemical performance of the LSC cathode at the intermediate-temperature with few reported studies in the literature (Table 2) is practically acceptable. Han *et al.* [18] used a commercial inkjet printer as a cell fabrication technique and proved that a simple and cost-effective technique can produce a $La_{0.6}Sr_{0.4}Co_{0.2}Fe_{0.8}O_{3-\delta}$ (LSCF) cathode with high electrochemical performance. Therefore, the simple G-S assisted with brush painting can still be regarded as a promising technique to fabricate LSC electrodes for intermediate-temperature PCFC application in a small-scale laboratory. The present results can be further improved by prolonging the grinding and stirring time and subjection to ultra-sonication to produce the improved and homogenized S1 cathode slurry [24–26]. However, the advanced BM-TRM technique assisted with screen printing is the ideal technique because it can enhance the electrochemical properties of the screen printed LSC cathode.

IV. Conclusions

A single-phase LSC cathode powder with the particle size of $0.28 \pm 0.06\,\mu m$ and specific surface area of $8.7\,m^2/g$ was synthesized via a sol-gel method at the calcination temperature of 900 °C. The present study demonstrated that the electrochemical performance of the prepared LSC cathode working on BCZY proton conductor for PCFC application can be improved by applying a combination of promising cell fabrication techniques such as slurry preparation and slurry deposition to produce the cathode layer. The advanced BM-TRM assisted with screen printing is a better cell fabrication technique than the simple G-S assisted with brush painting to produce high-performance LSC cathode. The ASR values of the LSC cathodes fabricated by the advanced and simple cell fabrication techniques measured at the operating temperature of 700 °C using the symmetrical cells of LSC|BCZY|LSC were $0.25\,\Omega\,cm^2$ and $1.50\,\Omega\,cm^2$, respectively. The electrochemical performance of the LSC cathode fabricated by the BM-TRM assisted with screen printing can be further improved by tailoring the microstructure properties of the LSC powder and the thickness of the LSC film.

Acknowledgement: The authors would like to acknowledge the Research University Grant (DIP-2016-005) provided by the Universiti Kebangsaan Malaysia (UKM) and the Ministry of Higher Education (MOHE) of Malaysia for the financial support provided via the Transdisciplinary Research Grant Scheme (600-IRMI/TRGS 5/3 (1/2016)-2). Abdullah Abdul Samat thankfully acknowledges the MOHE and the Universiti Malaysia Perlis (UniMAP) for the SLAB/SLAI PhD scholarship. The facility support from the Centre for Research and Instrumentation Management (CRIM) of UKM, Universiti Tun Hussein Onn Malaysia (UTHM) and Universiti Teknologi MARA (UiTM) is also gratefully acknowledged.

References

1. A. Subardi, C.C. Chen, Y.P. Fu, "Oxygen transportation, electrical conductivity and electrochemical properties of layered perovskite $SmBa_{0.5}Sr_{0.5}Co_2O_{5-\delta}$", *Int. J. Hydrog. Energy*, **42** [8] (2017) 5284–5294.
2. L. Zhang, C. Li, "$BaFe_{0.6}Co_{0.3}Ce_{0.1}O_{3-\delta}$ as cathode materials for proton-conducting solid oxide fuel cells", *Ceram. Int.*, **42** [8] (2016) 10511–10515.
3. O. Gwon, S. Yoo, J. Shin, G. Kim, "Optimization of $La_{1-x}Sr_xCoO_{3-\delta}$ perovskite cathodes for intermediate temperature solid oxide fuel cells through the analysis of crystal structure and electrical properties", *Int. J. Hydrog. Energy*, **39** [35] (2014) 20806–20811.
4. Z. Liu, M. Liu, L. Nie, M. Liu, "Fabrication and characterization of functionally-graded LSCF cathodes by tape casting", *Int. J. Hydrog. Energy*, **38** [2] (2013) 1082–1087.
5. L. Zhang, W. Long, F. Jin, T. He, "Electrical conductivity, thermal expansion and electrochemical performances of Ba-doped $SrCo_{0.9}Nb_{0.1}O_{3-\delta}$ cathodes for IT-SOFCs", *Int. J. Hydrog. Energy*, **38** [19] (2013) 7947–7956.
6. Y. Tao, J. Shao, J. Wang, W.G. Wang, "Synthesis and properties of $La_{0.6}Sr_{0.4}CoO_{3-\delta}$ nanopowder", *J. Power Sources*, **185** [2] (2008) 609–614.
7. A. Heel, P. Holtappels, T. Graule, "On the synthesis and performance of flame-made nanoscale $La_{0.6}Sr_{0.4}CoO_{3-\delta}$ and its influence on the application as an intermediate temperature solid oxide fuel cell cathode", *J. Power Sources*, **195** [19] (2010) 6709–6718.
8. J. Hayd, L. Dieterle, U. Guntow, D. Gerthsen, E. Ivers-

Tiffée, "Nanoscaled $La_{0.6}Sr_{0.4}CoO_{3-\delta}$ as intermediate temperature solid oxide fuel cell cathode: Microstructure and electrochemical performance", *J. Power Sources*, **196** [17] (2011) 7263–7270.
9. M.S. Wang, J.X. Wang, C.R. He, Y.J. Xue, H. Miao, Q. Wang, W.G. Wang, "A novel composite cathode $La_{0.6}Sr_{0.4}CoO_{3-\delta}$–$BaZr_{0.1}Ce_{0.7}Y_{0.1}Yb_{0.1}O_{3-\delta}$ for intermediate temperature solid oxide fuel cells", *Ceram. Int.*, **41** [3] (2015) 5017–5025.
10. A. Abdul Samat, M.R. Somalu, A. Muchtar, O.H. Hassan, N. Osman, "LSC cathode prepared by polymeric complexation method for proton-conducting SOFC application", *J. Sol-Gel Sci. Technol.*, **78** [2] (2016) 382–393.
11. Q. Shao, W.J. Ge, X. Lu, Y. Chen, Y. Ding, B. Lin, Y. Ling, "A promising cathode for proton-conducting intermediate temperature solid oxide fuel cells: $Y_{0.8}Ca_{0.2}BaCo_4O_{7+\delta}$", *Ceram. Int.*, **41** [5] (2015) 6687–6692.
12. B. Peng, G. Chen, J. Wang, J. Zhou, J. Guo, Y. Cheng, K. Wu, "Hydride reduced $LaSrCoO_{4-\delta}$ as new cathode material for $Ba(Zr_{0.1}Ce_{0.7}Y_{0.2})O_3$ based intermediate temperature solid oxide fuel cells", *J. Power Sources*, **201** (2012) 174–178.
13. S. Yoo, J. Kim, S.Y. Song, D.W. Lee, J. Shin, K.M. Ok, G. Kim, "Structural, electrical and electrochemical characteristics of $La_{0.1}Sr_{0.9}Co_{1-x}Nb_xO_{3-\delta}$ as a cathode material for intermediate temperature solid oxide fuel cells", *RSC Adv.*, **4** [36] (2014) 18710–18717.
14. S. Ricote, N. Bonanos, P.M. Rørvik, C. Haavik, "Microstructure and performance of $La_{0.58}Sr_{0.4}Co_{0.2}Fe_{0.8}O_{3-\delta}$ cathodes deposited on $BaCe_{0.2}Zr_{0.7}Y_{0.1}O_{3-\delta}$ by infiltration and spray pyrolysis", *J. Power Sources*, **209** (2012) 172–179.
15. N.S. Choi, Y.G. Lee, J.K. Park, "Effect of cathode binder on electrochemical properties of lithium rechargeable polymer batteries", *J. Power Sources*, **112** [1] (2002) 61–66.
16. D. Munao, J.W.M. van Erven, M. Valvo, E. Garcia-Tamayo, E.M. Kelder, "Role of the binder on the failure mechanism of Si nano-composite electrodes for Li-ion batteries", *J. Power Sources*, **196** [16] (2011) 6695–6702.
17. Z. Liu, M.F. Han, W.T. Miao, "Preparation and characterization of graded cathode $La_{0.6}Sr_{0.4}Co_{0.2}Fe_{0.8}O_{3-\delta}$", *J. Power Sources*, **173** [2] (2007) 837–841.
18. G.D. Han, K.C. Neoh, K. Bae, H.J. Choi, S.W. Park, J.W. Son, J.H. Shim, "Fabrication of lanthanum strontium cobalt ferrite (LSCF) cathodes for high performance solid oxide fuel cells using a low price commercial inkjet printer", *J. Power Sources*, **306** (2016) 503–509.
19. S.A. Muhammed Ali, M. Anwar, N.A. Baharuddin, M.R. Somalu, A. Muchtar, "Enhanced electrochemical performance of LSCF cathode through selection of optimum fabrication parameters", *J. Solid State Electrochem.*, **22** [1] (2018) 263–273.
20. M.R. Somalu, A. Muchtar, W.R.W. Daud, N.P. Brandon, "Screen-printing inks for the fabrication of solid oxide fuel cell films: A review", *Renew. Sustain. Energy Rev.*, **75** (2017) 426–439.
21. M.R. Somalu, V. Yufit, I.P. Shapiro, P. Xiao, N.P. Brandon, "The impact of ink rheology on the properties of screen-printed solid oxide fuel cell anodes", *Int. J. Hydrog. Energy*, **38** [16] (2013) 6789–6801.
22. M.R. Somalu, N.P. Brandon, "Rheological studies of nickel/scandia-stabilized-zirconia screen printing inks for solid oxide fuel cell anode fabrication", *J. Am. Ceram. Soc.*, **95** [4] (2012) 1220–1228.
23. H. Oda, T. Yoneda, T. Sakai, Y. Okuyama, H. Matsumoto, "Preparation of nano-structured cathode for protonic ceramic fuel cell by bead-milling method", *Solid State Ion.*, **262** (2014) 388–391.
24. F. Wei, H. Cao, X. Chen, "$La_{0.6}Sr_{0.4}CoO_{3-\delta}$–$Ce_{0.8}Gd_{0.2}O_{2-\delta}$ nanocomposites prepared by a sol-gel process for intermediate temperature solid oxide fuel cell cathode applications", *J. Mater. Sci.*, **51** [4] (2016) 2160–2167.
25. H. Lee, I. Park, J. Park, G. Lee, D. Shin, "Effects of dual porosity honeycomb structure in SSC-SDC composite cathode for SOFCs", *Int. J. Hydrog. Energy*, **40** [35] (2015) 11998–12002.
26. Y. Hu, Y. Bouffanais, L. Almar, A. Morata, A. Tarancon, G. Dezanneau, "$La_{2-x}Sr_xCoO_{4-\delta}$ (x = 0.9, 1.0, 1.1) Ruddlesden-Popper-type layered cobaltites as cathode materials for IT-SOFC application", *Int. J. Hydrog. Energy*, **38** [7] (2013) 3064–3072.
27. M.R. Somalu, A. Muchtar, N.P. Brandon, "Properties of screen-printed nickel/scandia-stabilized-zirconia anodes fabricated using rheologically optimized inks during redox cycles", *J. Mater. Sci.*, **52** [12] (2017) 7175–7185.
28. S.A. Muhammed Ali, M. Anwar, M.R. Somalu, A. Muchtar, "Enhancement of the interfacial polarization resistance of $La_{0.6}Sr_{0.4}Co_{0.2}Fe_{0.8}O_{3-\delta}$ cathode by microwave-assisted combustion method", *Ceram. Int.*, **43** [5] (2017) 4647–4654.
29. N.A. Abdullah, N. Osman, S. Hasan, O.H. Hassan, "Chelating agents role on thermal characteristics and phase formation of modified cerate-zirconate via sol-gel synthesis route", *Int. J. Electrochem. Sci.*, **7** (2012) 9401–9409.
30. M. Anwar, S.A. Muhammed Ali, A.M. Abdalla, M.R. Somalu, A. Muchtar, "Effect of sintering temperature on the microstructure and ionic conductivity of $Ce_{0.8}Sm_{0.1}Ba_{0.1}O_{2-\delta}$ electrolyte", *Process. Appl. Ceram.*, **11** [1] (2017) 67–74.
31. N.P. Bansal, Z. Zhong, "Combustion synthesis of $Sm_{0.5}Sr_{0.5}CoO_{3-x}$ and $La_{0.6}Sr_{0.4}CoO_{3-x}$ nanopowders for solid oxide fuel cell cathodes", *J. Power Sources*, **158** [1] (2006) 148–153.
32. M. Ghouse, Y. Al-Yousef, A. Al-Musa, M.F. Al-Otaibi, "Preparation of $La_{0.6}Sr_{0.4}Co_{0.2}Fe_{0.8}O_3$ nanoceramic cathode powders for solid oxide fuel cell (SOFC) application", *Int. J. Hydrog. Energy*, **35** [17] (2010) 9411–9419.
33. Y.C. Wu, P.Y. Huang, G. Xu, "Properties and microstructural analysis of $La_{1-x}Sr_xCoO_{3-\delta}$ (x = 0–0.6) cathode materials", *Ceram. Int.*, **43** [2] (2017) 2460–2470.
34. C. Benel, A.J. Darbandi, R. Djenadic, A. Evans, R. Tolke, M. Prestat, H. Hahn, "Synthesis and characterization of nanoparticulate $La_{0.6}Sr_{0.4}CoO_{3-\delta}$ cathodes for thin-film solid oxide fuel cells", *J. Power Sources*, **229** (2013) 258–264.
35. Y. Ling, F. Wang, L. Zhao, X. Liu, B. Lin, "Comparative study of electrochemical properties of different composite cathode materials associated to stable proton conducting $BaZr_{0.7}Pr_{0.1}Y_{0.2}O_{3-\delta}$ electrolyte", *Electrochimica Acta*, **146** (2014) 1–7.
36. Q. Su, S. Cho, Z. Bi, A. Chen, H. Wang, "Enhanced electrochemical properties of bi-layer $La_{0.5}Sr_{0.5}CoO_{3-\delta}$ cathode prepared by a hybrid method", *Electrochimica Acta*,

56 [11] (2011) 3969–3974.
37. L. Zhao, B. He, J. Gu, F. Liu, X. Chu, C. Xia, "Reaction model for cathodes cooperated with oxygen-ion conductors for solid oxide fuel cells using proton-conducting electrolytes", *Int. J. Hydrog. Energy*, **37** [1] (2012) 548–554.
38. N. Hedayat, Y. Du, H. Ilkhani, "Review on fabrication techniques for porous electrodes of solid oxide fuel cells by sacrificial template methods", *Renew. Sustain. Energy Rev.*, **77** (2017) 1221–1239.
39. L.S. Mahmud, A. Muchtar, M.R. Somalu, "Challenges in fabricating planar solid oxide fuel cells: A review", *Renew. Sustain. Energy Rev.*, **72** (2017) 105–116.
40. C. Loho, R. Djenadic, P. Mundt, O. Clemens, H. Hahn, "On processing-structure-property relations and high ionic conductivity in garnet-type $Li_5La_3Ta_2O_{12}$ solid electrolyte thin films grown by CO_2-laser assisted CVD", *Solid State Ionics*, **313** (2017) 32–44.
41. F. Zhao, R. Peng, C. Xia, "LSC-based electrode with high durability for IT-SOFCs", *Fuel Cells Bull.*, **2008** [2] (2008) 12–16.
42. I. Garbayo, V. Esposito, S. Sanna, A. Morata, D. Pla, L. Fonseca, N. Sabate, A. Tarancon, "Porous $La_{0.6}Sr_{0.4}CoO_{3-\delta}$ thin film cathodes for large area micro solid oxide fuel cell power generators", *J. Power Sources*, **248** (2014) 1042–1049.